Author/s:
Khor, SY;Vu, MN;Pilkington, EH;Johnston, APR;Whittaker, MR;Quinn, JF;Truong, NP;Davis, TP

Title:
Elucidating the Influences of Size, Surface Chemistry, and Dynamic Flow on Cellular Association of Nanoparticles Made by Polymerization-Induced Self-Assembly

Date:
2018-08-23

Citation:
Khor, S. Y., Vu, M. N., Pilkington, E. H., Johnston, A. P. R., Whittaker, M. R., Quinn, J. F., Truong, N. P. & Davis, T. P. (2018). Elucidating the Influences of Size, Surface Chemistry, and Dynamic Flow on Cellular Association of Nanoparticles Made by Polymerization-Induced Self-Assembly. Small, 14 (34), https://doi.org/10.1002/smll.201801702.

DOI: 10.1002/ ((please add manuscript number))

Article type: Full Paper

Elucidating the influences of size, surface chemistry and dynamic flow on cellular association of nanoparticles made by polymerization-induced self-assembly

Song Yang Khor‡, Mai N. Vu‡, Emily H. Pilkington, Angus P.R. Johnston, Michael R. Whittaker, John F. Quinn, Nghia P. Truong, and Thomas P. Davis**

S. Y. Khor‡, M. N. Vu‡, E. H. Pilkington, Dr. Angus P.R. Johnston, Dr. M. R. Whittaker, Dr. J. F. Quinn, Dr. N. P. Truong, Prof. T. P. Davis

ARC Centre of Excellence in Convergent Bio-Nano Science and Technology

Monash Institute of Pharmaceutical Sciences

Monash University

381 Royal Parade, Parkville, VIC 3052, Australia

E-mail: nghia.truong@monash.edu, thomas.p.davis@monash.edu

Prof. T. P. Davis

Department of Chemistry

University of Warwick

Gibbet Hill, Coventry CV47AL, UK

Keywords: dynamic flow, size, surface chemistry, cellular association, PISA

The size and surface chemistry of nanoparticles dictate their interactions with biological systems. However, it remains unclear how these key physicochemical properties affect the cellular association of nanoparticles under dynamic flow conditions encountered in human vascular networks. Here we report the facile synthesis of novel fluorescent nanoparticles with tunable sizes and surface chemistries and their association with primary human umbilical vein endothelial cells (HUVECs). First, we developed a one-pot polymerization-induced self-assembly (PISA) methodology to covalently incorporate a commercially available fluorescent dye into the nanoparticle core and tuning nanoparticle size and surface chemistry. To characterize cellular association under flow, HUVECs were cultured onto the surface of a synthetic microvascular network embedded in a microfluidic device (SynVivo, INC). Interestingly, increasing the size of carboxylic acid-functionalized nanoparticles led to the higher cellular association under static conditions but lower cellular association under flow conditions. Whereas increasing the size of tertiary amine-decorated nanoparticles resulted in a higher level of cellular association, under both static and flow conditions. These findings provide new insights into the interactions between polymeric nanomaterials and endothelial cells. Altogether, this work establishes innovative methods for the facile synthesis and biological characterization of polymeric nanomaterials for various potential applications.

1. Introduction

Polymeric nanomaterials hold great potential for improving the diagnosis and treatment of diseases with reduced off-target effects.[1-2] The encapsulation of drugs and imaging agents inside the core of nanomaterials has been shown to improve drug efficacy and imaging contrast by enhancing *in vivo*

solubility, stability, and targeting.[3-4] This encapsulation also reduces peripheral toxicity and cardiotoxicity that would otherwise be encountered during the circulation of these compounds around the cardiovascular system.[5] Moreover, antibodies covalently attached to the surface of nanoparticles are able to trigger the immune responses against bacteria, viruses and cancer cells more effectively than free antibodies.[6] In cardiovascular diseases, nanoparticles decorated with targeting ligands have been increasingly exploited for the delivery of therapeutics to the vascular wall (i.e., endothelial cells).[7]

For the above clinical applications, nanomaterials circulate in the human vascular network before reaching their targets (e.g., cancer cells, immune cells, or blood clots).[8] As such, investigating and understanding the complex nano-bio interactions between nanomaterials and biological systems inside vascular networks (e.g., endothelial cell adhesion) are critical for designing nanoparticles with desired properties for these applications.[9] For instance, nanoparticles carrying anti-cancer drugs are expected to have a minimal off-target association with healthy endothelial cells before reaching tumors.[10] On the other hand, specific association between nanomaterials and endothelial cells may be beneficial for use in cardiovascular diseases.[9] Despite these potential benefits, the interactions between nanomaterials and endothelial cells under flow conditions in vascular networks remain poorly characterized due to a lack of suitable models.[11]

A major challenge in the *in vitro* characterization of interactions between nanomaterials and endothelial cells is to mimic dynamic flow conditions and complex microenvironments that exist within *in vivo* vascular networks.[12-13] Traditional approaches for studying nano-bio interactions typically involve incubating nanoparticles with cells under static conditions (e.g., in a well-plate), which clearly fails to model dynamic flow conditions in the vascular network.[14] Considerable efforts have been made to develop reliable methods for evaluating cellular associations of nanomaterials

under realistic flow conditions. For example, Langer and coworkers have developed a simple microfluidic device lined with cells as a tool for determining parameters that affect cellular interaction of nanoparticles under flow conditions.[15] This device was prepared by using electrical tape to attach a polydimethylsiloxane (PDMS) mould onto a glass slide to create a single, straight microchannel (54 x 900 μm). Samuel and colleagues have employed a more complex microfluidic device with multichannels to evaluate cellular uptake of silica particles into endothelial cells.[16] This work highlighted that shear stress and surface chemistry are critical parameters for nanoparticle uptake by endothelial cells.[16] To date, the majority of studies in nano-bio interactions under flow conditions employ microfluidic devices with simple straight microchannels, which do not adequately reflect the complex geometry and dynamic shear rates found in vascular networks.

Recent advances in computer-aided lithography have enabled the manufacture of microfluidic devices with vascular network mimicking channels. In particular, Prabhakarpandian and coworkers have successfully developed physiologically realistic synthetic microvascular networks (SMNs) for modeling cell-cell and particle-cell interactions in the microvasculature.[17-18] These SMNs not only possess a complex geometry similar to microvasculature but also can mimic various shear rates observed *in vivo*.[19-20] Mitragotri and colleagues have employed these SMNs to explore the effects of nanoparticle shape and flow on targeting antibody-coated nanoparticles to lung and brain endothelium.[21-22] Moreover, variants of the SMN have been developed which incorporate both a SMN and a tumor region, thus allowing rapid screening of cancer drug delivery systems.[23-24] So far, these realistic SMNs have been employed to investigate the effect of only single physicochemical property of polymeric nanomaterials (e.g., size or surface chemistry alone) on nano-bio interactions under flow conditions. As such, we still do not understand how the nano-bio interactions in vascular networks will change with systematic variation of multiple nanoparticle physicochemical properties

(e.g., both size and surface chemistry). In order to gain such understanding, it is necessary to reproducibly synthesize a comprehensive library of fluorescently labeled polymeric nanoparticles with various surface chemistries and similar size, as well as various sizes and identical surface chemistry.[25]

We have recently developed several reversible addition-fragmentation chain transfer (RAFT) emulsion polymerization techniques that can be used to synthesize nanoparticles with tunable size, shape, and surface chemistry via either polymerization-induced self-assembly (PISA) or temperature-induced morphological transformation (TIMT).[26-30] Emulsion polymerization is an environmentally and industrially friendly technique that can be used to reproducibly yield large-scale, concentrated nanoparticle suspensions in water.[31-32] Significantly, PISA can be employed to prepare nanoparticles with various sizes (diameters) and identical surface chemistry by using a single macromolecular chain transfer agent (macro-CTA) and different amount of a hydrophobic monomer (i.e., styrene).[33] The diameters of these PISA nanoparticles could be predetermined before the polymerization, thus allowing the reproducible production of nanoparticles with the desired size. However, modification of the macro-CTA end group typically resulted in a change in the morphology of PISA nanoparticles (from sphere to worm and vesicle).[34] As such, it remains challenging to prepare spherical nanoparticles with different surface chemistries and similar size via the PISA technique. Additionally, the core of PISA nanoparticles has not been labeled with a commercially available fluorescent dye, thus limiting their applications in nano-bio interaction studies.

To address these synthesis challenges, we developed a PISA formulation for the production of fluorescently labeled spherical nanoparticles that have the same size and various surface chemistries as well as the identical surface chemistry and different sizes. This PISA technique allowed the facile preparation of a library of 12 nanoparticles (4 surface chemistries × 3 sizes). These nanoparticles were

fluorescently labeled with a commercially available Cyanine5 maleimide (Cy5-maleimide, Lumiprobe) to allow the subsequent studies of nano-bio interactions. To characterize the association of these nanoparticles with endothelial cells under flow conditions, HUVECs were cultured under cell medium flow in vascular network microchannels of a microfluidic chip (SynVivo). After the HUVECs became confluent, fluorescently labeled nanoparticles were injected into the vascular network channels using a syringe pump. Subsequently, the HUVECs were collected and analyzed using flow cytometry and confocal microscopy. Interestingly, data obtained revealed for the first time the interplay of size, surface chemistry and flow conditions in the cellular association of PISA nanoparticles.

2. Results and Discussion

2.1. Synthesis of PISA nanoparticles having various surface chemistries and a predetermined diameter

First, we modified the carboxylic acid group of 4-cyano-4-(ethylthiocarbonothioylthio) pentanoic acid (ECT) with methanol (Me), dimethylamino-1-propanol (TA) and poly(ethylene glycol) methyl ether (PEG) (**Scheme 1**A) to produce three new CTAs with different functional groups (ECT-Me, ECT-TA, and ECT-PEG, respectively). ^{1}H NMR spectra (Figure S1) confirm the successful synthesis of these CTAs. Four CTAs (including ECT) were subsequently employed in RAFT solution polymerization of PEGA and HEAA using ACPA as a radical initiator (Scheme 1B). It is worth noting that a low ACPA/CTA ratio (5 mol% instead of 10%) was judiciously selected to produce well-defined macro-CTAs with high end-group fidelity.[34] In this work, the high end-group fidelity of macro-CTAs plays an important role because these end groups introduce different surface chemistries (a pre-modification approach). After purification, well-defined macro-CTAs with four different end groups were obtained. In contrast to the different end groups, these macro-CTAs exhibit similar

compositions and molecular weights (Table S1), which is expected to facilitate reproducible access to PISA nanoparticles with predetermined sizes.[33] That said, the difference in macro-CTA end group has been found to affect the morphology of nanoparticles obtained by the PISA technique.[34] As such, it is challenging to prepare spherical nanoparticles with different surface chemistries using PISA technique.

To address this challenge, a low ACPA/macro-CTA ratio (12 mol%) was chosen for RAFT emulsion polymerization of styrene. In our previous work, when employing a macro-CTA terminated with a methyl ester group, it has been demonstrated that this low ACPA/macro-CTA ratio resulted in a reduced number of polymer chains aggregating during the initial phase of the PISA process and the formation of PISA nanoparticles having a spherical morphology.[34] In this work, we hypothesized that using this low ratio of ACPA/macro-CTA (12 mol%) would also lead to only spherical PISA nanoparticles, regardless of macro-CTAs having four different end groups. To test this hypothesis, four emulsion polymerizations of styrene using 12 mol% of ACPA/macro-CTA ratio and macro-CTAs with carboxylic acid (COOH), methyl ester (Me), tertiary amine ester (TA), and PEG end groups were conducted. After the emulsion polymerizations, the morphology of nanoparticles was characterized by TEM. Figure S4 shows that all nanoparticles with different surface chemistries exhibited the same spherical shape and relatively similar size, regardless of macro-CTAs end groups. This supports our hypothesis and demonstrates for the first time that PISA technique, in addition to its well-known capacity to tune particles size and shape, can also be used to prepare spherical nanoparticles with various surface chemistries and predetermined particle sizes.

2.2. A novel PISA method to label nanoparticles with a commercially available fluorescent dye

To label PISA nanoparticles with fluorescent dyes, there are several techniques available in the literature. For instance, Armes and coworkers have developed a post-modification method to label the

surfaces of PISA nanoparticles with rhodamine dyes using thiol chemistry.[35] The presence of rhodamine dyes on the surface may affect the cellular association of PISA nanoparticles and therefore, this approach is not suitable for this study. To label the core of PISA nanoparticles with fluorescent dyes, Clavier and colleagues synthesized a family of boron-dipyrromethene (BODIPY) monomers.[36] This method can covalently attach fluorescent dyes in the core of PISA nanoparticles during emulsion polymerization. However, these BODIPY monomers are not commercially available and this method is limited to a small number of fluorescent dyes. To develop a more facile and versatile technique, we selected Cy5-maleimide as a representative for a large family of commercially available fluorescent dyes having a maleimide functional group. It has been shown that *N*-substituted maleimides rapidly insert into growing polystyrene chains allowing the precise incorporation of N-substituted maleimide units in these polymers.[37-38] As such, we hypothesized that *N*-substituted Cy5-maleimide dye could rapidly copolymerize with styrene during the PISA process, even in the presence of a high excess of styrene (Scheme 1C). To verify this hypothesis, Cy5-maleimide in styrene was added after 4 h emulsion polymerization of styrene (when the solution became turbid indicating PISA nanoparticles formed). After another 2 h of polymerization followed by purification by dialysis, the polymer product was characterized by SEC coupled with refractive index (RI) and UV-Vis detectors. SEC traces from RI and UV-Vis detectors in Figure S5 revealed two peaks at a relatively similar retention time at approximately 26 mins, suggesting that the Cy5 dye had been covalently incorporated into the polystyrene chains (the core of PISA nanoparticles). This PISA method (the addition of maleimide dyes during PISA process) paves the way for the facile and versatile labeling of PISA nanoparticles with commercially available fluorescent dyes.

We employed this newly developed PISA method to prepare a library of 12 fluorescently labelled nanoparticles for nano-bio interaction studies (**Figure 1**). The nanoparticle library consists of three

sizes (small: ~40 nm, medium: ~70 nm, and large: ~130 nm) and four surface chemistries (carboxylic acid: COOH, tertiary amine: TA, methyl ester: Me and PEG). The sizes of nanoparticles were precisely determined before the polymerization by targeting different molecular weights (Figure S6 to S9).[33] This allows us to produce PISA nanoparticles with relatively similar sizes (see TEM images in Figure 1) and low dispersity (below 0.2, see DLS data in Table S2 to S5) even though four different macro-CTAs were used. The surface chemistries of nanoparticles were changed by modifying the CTAs as discussed above. It should be noted that altering the surface chemistries of the nanoparticles did not result in any appreciable differences in zeta potential (Table S2 to S5). Nonetheless, this pre-modification approach allows us to estimate the percentage of functional groups available on the surface of PISA nanoparticles as previously described.[34] Significantly, all nanoparticles have been successfully labelled with Cy5 dyes (Figure S11). Altogether, we have synthesized the first library of fluorescently labelled, spherical PISA nanoparticles that have tunable sizes and surface chemistries.

2.3. Toxicity of macro-CTAs and PISA nanoparticles

After polymerization, the macro-CTAs were precipitated to remove unreacted monomer and then extensively dried in a vacuum oven to remove trace amounts of organic solvent. The nanoparticles were dialyzed against MiliQ water for 48 h to remove unreacted styrene monomer confirmed via the absence of styrene vinyl peaks on the ^{1}H NMR spectrum (Figure S2). Before the nano-bio interaction studies, the toxicity of all macro-CTAs and nanoparticles was investigated. We used AlamarBlue assays for characterization of cell viability of HUVECs because the fluorescent emission of AlamarBlue reagents (610 nm) does not overlap with that of Cy5 dye (680 nm) attached in the styrenic core of PISA nanoparticles. Cell viability data in **Figure 2** suggest that all macro-CTAs and nanoparticles are well-tolerated, even at high concentrations up to 1 mg mL^{-1}. Only small- and medium-size nanoparticles with tertiary amine groups on the surface (S4 and M4) and medium-size

nanoparticles with Me and PEG surface (M2 and M3) exhibited slight toxicity (cell viability reduced to approximately 80%), which may be related to high level of cellular associations of these nanoparticles (see data and discussion below). To minimize the potential impact of toxicity on understanding nano-bio interactions, we used nanoparticle concentrations in the range 10 to 200 μg mL^{-1} for all subsequent cellular association studies in both static and flow conditions.

2.4. Preparation of synthetic microvascular networks in a microfluidic device

One of the major challenges in the preparation of the synthetic microvascular networks is the formation of a confluent and intact lumen of HUVECs in PDMS microchannels of a microfluidic device (SynVivo, see **Figure 3**A). To address this challenge, these microchannels were first coated with Matrigel®, a "glue" for attachment of HUVECs onto the PDMS surface. This step was conducted under cold conditions (all reagents and the microfluidic chips were stored in the fridge and kept in an ice bath during the coating) to minimize the polymerization of Matrigel® and the formation of clumps. That said, we found that some clumps still formed, but could be removed by extensive washing with endothelial cell growth medium (EGM). It is worth noting that prior removal of any Matrigel® clump is important for the subsequent formation of a complete and confluent layer of HUVECs inside the microchannels. After coating with Matrigel®, HUVECs (2.5×10^7 cells mL^{-1}) were slowly injected until they covered approximately 90% of the surface of the microchannels (see Figure S10). The chip was then placed in an incubator (37 °C, 5% CO_2) for 1 h to allow cells to attach to the Matrigel®-coated microchannel surface. Subsequently, fresh EGM at 37 °C was injected into the microchannel at a flow rate of 0.1 μL min^{-1}. After 24 h, a complete and confluent layer of HUVECs was observed by both bright field and confocal microscopy (Figure 3B and 3C). It has been demonstrated that endothelial cells cultured under such flow conditions have the similar morphology and function to that observed *in vivo*.[23,39] To further verify the complete formation of a three dimensional (3D) lumen of

HUVECs on the top, bottom, and side of the microchannels, an Eclipse TiE Microscope with a Nikon A1R Confocal was utilized to acquire a 3D Z-stack of the synthetic vessels. Figure 3D, 3E, and 3F show images of the cell nucleus stained with Hoechst 33342 (a stain that emits blue fluorescence when bound to dsDNA in the cell nucleus) when focused at the bottom, at the top, and on the sides of microchannels, respectively. These images confirm the formation of a complete lumen of HUVECs under flow conditions and suggest that the microfluidic chip is ready for use as a synthetic microvascular network (Video S1).

2.5. Effects of dynamic flow conditions on PISA nanoparticles with different surface chemistries

After the microfluidic chip was successfully coated with HUVECs, nanoparticle suspension in EGM (at 37 °C) was introduced into the synthetic microvascular network at a flow rate of 1.0 μL min^{-1}. This flow rate was selected to create a physiological shear rate range (from ~ 30 to ~ 240 s^{-1}) found *in vivo*.[19,23] After 4 h, chilled HBSS was injected to remove non-associated nanoparticles from the microchannels before HUVECs were collected for analysis by flow cytometry. The concentration of nanoparticles in all studies was kept constant at approximate 1 x 10^{11} particles mL^{-1} (measured by Nanosight) to ensure the same number of nanoparticles were interacting with HUVECs in each experiment. We also performed cellular association studies under static conditions (where PISA nanoparticles were incubated with HUVECs in 48-well plates) at the same concentration to ensure that data obtained under static and flow conditions were comparable.

Figure 4 shows the median fluorescence intensity (MFI) of Cy5 dye detected by flow cytometry, which indicates the level of PISA nanoparticles (medium size ~ 70 nm) associated with HUVECs. The fluorescence intensity of all nanoparticles was slightly different (Figure S11) and therefore, these MFI values in Figure 4 were normalized to the same fluorescent intensity per nanoparticle. Data in Figure 4 demonstrated that the level of nanoparticles associated with HUVECs in flow conditions was

significantly reduced when compared to static conditions. Specifically, for COOH-, PEG-, Me-, and TA-functionalized particles, the MFI values were decreased 4.27 ($P < 0.01$), 6.07 ($P < 0.0001$), 6.37 ($P < 0.001$), and 7.01 ($P < 0.001$) fold, respectively. The decreased association between nanoparticles and HUVECs under flow conditions may be related to the reduced exposure of these nanoparticles to cells even though the same number of particles had been introduced.[10] In flow conditions, spherical nanoparticles tend to follow the cell medium streamlines when passing through the synthetic microvascular networks while in static conditions, all nanoparticles have a tendency to settle on the cell surfaces due to gravity.[40] That said, the trend of association between HUVECs and PISA nanoparticles of different surface chemistries (i.e., COOH < PEG < Me < TA) is similar when comparing between static and flow conditions. This result suggested that studying nano-bio interactions of these PISA nanoparticles under static conditions may be still useful to predict interaction trends but cannot provide quantitative information on the level of cellular association under flow conditions.

Furthermore, under static and flow conditions, nanoparticles that possessed TA-terminated groups exhibited enhanced cellular association compared to COOH-functional nanomaterials. This result is consistent with previous studies and may be related to the adsorption of different proteins from the cell medium onto the nanoparticle surface formimg a protein corona.[41-44] Further work is needed to comprehensively investigate the protein corona of these PISA particles in the presence of cell media, serum and plasma. In the present study, we proceeded to further investigate the effect of dynamic flow conditions on the two types of PISA nanoparticles that exhibited the highest and lowest level of cellular associations (M4-TA and M1-COOH, respectively).

2.6. Effects of dynamic flow conditions on PISA nanoparticles with different sizes

In this study, we first investigated how dynamic flow conditions affected the degree of cellular association of TA-functionalized nanoparticles with various sizes. **Figure 5** shows that under both static and flow conditions, an increase in particle size led to an enhanced cellular association between TA-functionalized nanoparticles and HUVECs. Similar to the results for varying surface chemistry, data obtained in static condition could be used to predict the trend in cellular association as a function of particle size under flow conditions for TA-decorated nanoparticles. That said, the level of cellular association under flow conditions was significantly lower than was observed under static conditions, which may also be related to the reduced exposure as discussed above.

To observe the cellular association of TA-functionalized particles with HUVECs, cells were further stained with Hoechst 33342 and then imaged by a Nikon confocal microscope. Confocal microscopy images in **Figure 6** showed that large nanoparticles (130 nm) associated with HUVECs to a greater extent than medium and small particles (70 nm and 40 nm), which is consistent with data obtained by flow cytometry (Figure 5). It has been shown that large nanoparticles exhibit a higher tendency to tumble out of the general circulation and scavenge along vascular walls than smaller nanomaterials.[9, 45-46] This tendency may increase the exposure of large nanoparticles with TA-tagged groups to endothelial cells and as a result, increase cellular association. From Figure 6, it is unclear whether these nanoparticles are internalized into the cells or merely bound to the cell surface. To further interrogate this, we collected HUVECs, stained the cells with Calcein AM and Hoechst 33342 and acquired Z-stack images of these cells using a high-resolution confocal microscopy. Images in **Figure 7** and S13 suggest that TA-functionalized particles may be internalized by HUVECs. That said, additional characterization (e.g., using a specific hybridization internalization probe) are needed to fully confirm the cellular uptake of these particles.[47]

Next, the cellular association of carboxylic acid-decorated nanoparticles with three different sizes was studied. **Figure 8** shows that, under static conditions, the larger nanoparticles had a higher degree of cellular association than did the smaller particles (a similar trend to that observed for TA-functionalized nanoparticles). Interestingly, this trend is reversed under flow conditions. Small carboxylic acid-decorated nanoparticles exhibited the highest level of cellular association (approximately 9 fold higher than medium and large nanoparticles). As such, for carboxylic acid-decorated nanoparticles, data obtained in the static assay cannot be used to predict the trend in cellular associations under flow conditions. The decreased cellular association of medium and large nanoparticles decorated with carboxylic acid may be related to the effect of a strong drag force induced by the fluidic flow.[48] It has been postulated that drag force of the fluidic flow on large nanoparticles is higher than that on small particles and therefore, large nanoparticles are detached from cell surfaces more than small counterparts.[49-50] In the other words, the low drag force of fluidic flow exerted on the on 40-nm nanoparticles with carboxylic acid surfaces is not strong enough to detach these particles from the cell surface whereas the high drag force on medium and large nanoparticles is sufficient to detach these particles from HUVECs (Figure S14). For TA-functionalized nanoparticles, the effect of drag force (even on large nanoparticles) is negligible compared to their strong adhesive force with HUVECs and hence, the flow conditions cannot reverse the trend of cellular associations. Additionally, the cellular uptake of carboxylic acid-, PEG- and methyl- functionalized nanoparticles was observed by confocal microscopy (**Figure 9**, S12, and S15). Taken together, these results clearly indicate that the effect of flow conditions on cellular associations is strongly dependent not only on the particle size but also the particle surface chemistry.3. Conclusion

We have successfully developed a facile PISA method to label the core of nanoparticles with a commercially available fluorescent dye. This method simply exploits the rapidly polymerizable maleimide moiety commonly found in commercially available functional dyes. As such, this versatile method has great potential to be widely used for the reproducible preparation of large-scale, concentrated, and fluorescently labeled nanoparticles. By using a low ratio of radical initiator/macro-CTA ratio (12 mol%), the PISA nanoparticles remains spherical shape regardless of the end group, which allows the synthesis of a library of PISA nanoparticles having various sizes and identical surface chemistry as well as different surface chemistries and similar size. This library has enabled comprehensive investigation of the interplay of particle size, surface chemistry and flow conditions on particle associations with endothelial cells. Under both static and flow conditions, nanoparticles functionalized with TA groups associated with HUVECs more than particles with PEG, methyl ester and carboxylate surfaces. In contrast, carboxylic acid group decorated nanoparticles bind relatively weakly to HUVECs and as such, larger-sized particles (130 nm and 70 nm) are strongly affected by the drag force leading to removal from cell surfaces. We also found that assays under static conditions failed to predict behavior under flow for particles that bind weakly with HUVECs (i.e., for particles with COOH surfaces). Altogether, the synthesis and biological characterization methods developed in this work enable improved characterization of the nano-bio interactions of nanomaterials under flow conditions, and pave the way for future studies that will employ human blood as the mobile phase to more accurately mimic the human vascular network. Diverse particle parameters (such as size, shape, surface chemistry, rigidity, and targeting ligands) will also be studied to provide optimum nanoparticle designs for potential applications in drug delivery, immunotherapy, and cardiovascular disease treatments.

4. Experimental Section

Materials: Ethanethiol (97%), carbon disulfide (>99.9%), p-toluenesulfonyl chloride (>99%), dimethyl sulfoxide (>99.9%, anhydrous), dicyclohexylcarbodiimide (DCC), 4-dimethylaminopyridine (DMAP), trimethylamine (>99%), methanol (99%, anhydrous grade), 3-dimethylamino-1-propanol (TA, 99%), poly(ethylene glycol) methyl ether (PEG, average M_n=550), and p-toluenesulfonic acid monohydrate (>98.5%) were purchased from Sigma Aldrich and used as received. Cy5-maleimide was purchased from Lumiprobe and used as received. Poly(ethylene glycol) methyl ether acrylate (PEGA, average M_n=480 g mol^{-1}; Sigma-Aldrich), N-hydroxyethyl acrylamide (HEAA, 97%, Sigma-Aldrich), and styrene (>99%, Sigma-Aldrich) were passed through a column of basic aluminia (activity I) to remove inhibitor before use. 4,4'Azobis(4-cyanopentanoic acid) (ACPA, 98%, Alfa Aesar) was recrystallized twice in methanol before use. MiliQ water (resistivity > 18.2 MΩ cm^{-1}) was produced by a Millipore MiliQ Academic Water Purification System. All other chemicals and solvents used were of at least analytical grade and used as received.

Synthesis of chain transfer agents (CTAs): 4-cyano-4-(ethylthiocarbonothioylthio) pentanoic acid (ECT-COOH) was synthesized as previously described.[33] Modification of ECT-COOH with methanol (ECT-Me) was carried out as previously described.[34] Modification of ECT-COOH with TA (ECT-TA) and PEG (ECT-PEG) was conducted as follow: ECT-COOH (1.00 g, 3.8 mmol), DMAP (0.112 g, 0.38 mmol), and dimethylamino-1-propanol (0.450 mL of 0.872 g/mL, 3.8 mmol) or PEG (3.1 g, 5.7 mmol) were dissolved in anhydrous dichloromethane (8.0 mL), and added to a 50 mL round bottom flask equipped with a magnetic stirring bar, which was cooled in an ice bath. DCC (1.18 g, 5.7 mmol) was dissolved in anhydrous dichloromethane (8.0 mL) and slowly added dropwise over 5 min under stirring. The reaction vessel was then brought out of the ice bath and allowed to warm up to room temperature. After stirring continuously for 16 h, the reaction mixture was filtered twice to remove dicyclohexyl urea. The filtrate was dried over magnesium sulfate before purification by

column chromatography on silica gel. To purify ECT-TA, gradient solvent mixtures were used: petroleum benzine (boiling range 60-80 °C) : ethyl acetate (3 : 2 gradually changed to 1 : 2), and subsequently petroleum benzine (boiling range 60-80 °C) : ethyl acetate (1 : 1 with 5 v/v % triethylamine). After complete removal of residual solvents, a dark orange oil was obtained (0.823 g, 62% yield). To purify ECT-PEG, different gradient solvent mixtures were used: petroleum benzene : ethyl acetate (3 : 2 slowly changed to 1: 2) and subsequently, acetone. After complete removal of residual solvents, an orange oil was obtained (1.588 g, 51% yield). Characterization of the four CTAs by Nuclear Magnetic Resonance spectroscopy (NMR) is provided in Figure S1.

Synthesis of macro-CTAs: P(PEGA-*co*-HEAA)-COOH, P(PEGA-*co*-HEAA)-TA, P(HEAA-*co*-PEGA)-Me, and P(PEGA-*co*-HEAA)-PEG were synthesized as follows: ECT/ECT-TA/ECT-Me/ECT-PEG (120 mg/160 mg/126 mg/368 mg, 4.58 x 10^{-4} mol), PEGA (7.00 g, 1.46 x 10^{-2} mol), HEAA (2.10 g, 1.83 x 10^{-2} mol), ACPA (6 mg, 2.28 x 10^{-5} mol) and DMSO (48 mL, anhydrous) were added to a 50 mL round bottom flask equipped with a stirrer bar. The flask was sealed with a rubber septum and sparged with nitrogen for 1 h at room temperature. After polymerization for 4 h in an oil bath at 70 °C, the flask was cooled in an ice bath and exposed to air. Aliquots (50 µL) of the crude reactions were sampled for ^{1}H NMR and SEC analysis to determine PEGA and HEAA conversion, and polydispersity index (PDI). The crude reactions were dialyzed against acetone (1 L) using a dialysis membrane (MWCO = 3.5 kDa) for 3 h, to exchange the DMSO. The polymers were recovered via precipitation from acetone into a large excess of diethyl ether (300 mL) and dried under high vacuum for 48 h. Characterizations of the four macro-CTAs were provided in the supporting information (Table S1 and Figure S3).

Synthesis of fluorescently labeled nanoparticles: A typical emulsion polymerization of styrene and Cy5 maleimide was carried out as follows: macro-CTA (86 mg, 5.5×10^{-6} mol) was added to a 25 mL glass bottle equipped with a stirrer bar. ACPA (1.0 mg, 3.5×10^{-6} mol) was dissolved in MilliQ water (20 mL) by stirring for 30 min. A portion (4 mL) of that ACPA solution (3.5×10^{-4} mol L^{-1}) was mixed with the macro-CTA in the glass bottle and sealed with a rubber septum. Styrene (1 mL) was added to a 2 mL glass bottle and also sealed with a rubber septum. Both glass bottles were sparged with nitrogen for 25 min at room temperature. After that, an aliquot of deoxygenated styrene (400 µL) was added to the 25 mL glass bottle drop-wise via a gas-tight syringe. The reactants were purged for a further 5 min before heating in an oil bath preheated to 80 °C (stirring at 300 rpm). While polymerizing, Cy5 maleimide (1.0 mg, 1.6×10^{-6} mol) was added to 1 mL of styrene and stirred for 30 min in the dark at room temperature. The Cy5 maleimide/styrene mixture was then filtered through a 0.45 µm PTFE filter and then sealed with a rubber septum before sparging with nitrogen for 10 min. An aliquot (50 µL) of the Cy5 maleimide/styrene mixture was then added to the emulsion polymerization at 4 h via a gas-tight syringe. The polymerization was then allowed to continue for another 2 h before cooling the reaction in an ice bath and opening to the air. An aliquot (50 µL) of the crude mixture was sampled for SEC and ^{1}H NMR analysis. The reaction mixture was dialyzed against MilliQ water for 48 h using a dialysis membrane (MWCO= 12 kDa) and stored in the fridge (4 °C) and in the dark to prevent photobleaching. The fluorescence signal of each nanoparticle was characterized by fluorescence spectrophotometry (Figure S11).

Characterizations of CTAs, macro-CTAs, and nanoparticles: ^{1}H NMR spectroscopy: All ^{1}H NMR spectra were obtained in deuterated chloroform (RAFT agents), deuterated DMSO (macro-CTAs) or a mixture of deuterated acetone and deuterated chloroform in a 9 : 1 ratio (emulsion polymerizations) on a Bruker Advance III 400 MHz spectrometer. Size exclusion chromatography (SEC): Analyses of

polymer solutions were performed using a Shimadzu modular system comprising a DGU-12A degasser, an SIL-20AD automatic injector, a 5.0 μm bead-size guard column (50 x 7.8 mm) followed by three KF-805L columns (300 x 8 mm, bead size: 10 μm, pore size maximum: 5000 Å), a SPD-20A ultraviolet detector (the absorbance was set at 646 nm to detect Cy5), and an RID-10A differential refractive-index detector. A CTO-20A oven was used to maintain the columns at 40 °C. The eluent was *N*,*N*-dimethylacetamide (HPLC grade, with 0.03 % w/v LiBr) with a flow rate set at 1 mL min^{-1} using an LC-20AD pump. Calibration was done using commercial narrow molecular weight distribution polystyrene (PSTY) standards with a molecular weight range of 500 to 2 x 10^6 g mol^{-1}. All polymer samples were passed through a 0.45 μm PTFE filter prior to injection. Transmission electron microscopy (TEM): An aliquot (5 μL) of 0.1 wt% latex solution (diluted with MiliQ water) was deposited on a Formvar-coated copper grid (GSCu100F-50, Proscitech) and was left to dry overnight in the air and at room temperature. TEM imaging was performed using a Tecnai F20 transmission electron microscope at an accelerating voltage of 200 kV at ambient temperature. Dynamic light scattering (DLS): Dynamic light scattering measurements were performed using a Malvern Zetasizer Nano Series running DLS software and operating a 4 mW He–Ne laser at 633 nm. The analysis was performed at an angle of 173°. The sample refractive index (RI) was set at 1.59 for polystyrene. The dispersant viscosity and RI were set to 0.89 Ns m^2 and 1.33, respectively. The number of nanoparticles per 1 mL was measured using a NanoSight NS300 (Malvern). The measurements were carried out with nanoparticle solutions (0.1 μg/mL) at room temperature with manual shutter and gain adjustments. SEC, ^{1}H NMR, TEM, and DLS data for all nanoparticles are reported in the Supporting Information (COOH: Table S2, Figure S6, PEG: Table S3, Figure S7, Me: Table S4, Figure S8, TA: Table S5, Figure S9).

Cell viability assay: Cell viability studies were conducted in the presence of macro-CTAs and nanoparticles using the AlamarBlue assays. HUVECs (Lonza) were seeded onto 96-well plates at a cell density of 5,000 cells per well in 100 μL of endothelial cell growth medium (EGM, Lonza). The cells were then incubated at 37 °C, 5% CO_2 for 24 h. Subsequently, the medium was removed and replenished with 100 μL of fresh medium along with different concentrations of the polymers. After 48-hour incubation, the cells were washed twice with chilled HEPES buffered saline solution (HBSS, Sigma Aldrich) before being incubated with 10% (v/v) AlamarBlue reagent in EGM for 4 h at 37 °C, 5% CO_2. Fluorescence was measured at an excitation wavelength of 510 nm and an emission wavelength of 610 nm using a ClarioStar microplate reader. The experiments were performed in triplicate, and relative cell viability was calculated as the percentage viable compared to control cells in EGM without the addition of polymers and nanoparticles.

Culture of HUVECs in synthetic microvascular networks under cell medium flow: Before seeding HUVECs into the microvascular network device/chip (SynVivo, SMN1-D001), Matrigel® (Invitro Technologies) was used to coat microchannels inside the chip. First, Matrigel® (1/10 in chilled EGM) was injected into the device in cold conditions. After that, the chip was placed in a fridge at 4 °C for 1 h and then at 37 °C, 5% CO_2 in an incubator before a flow of fresh EGM were perfused through the chip to wash out unreacted Matrigel® and gel clumps. Next, HUVECs (2.5×10^7 cells mL^{-1}) were gently injected into the network until reaching 90% confluence (see Figure S10) before clamping the inlet and outlet ports. The device was then incubated (37 °C, 5% CO_2) for around 1 h for cell attachment before cell medium was changed. After that, a flow of fresh medium was perfused through the chip at the rate of 0.1 μl min^{-1} 20 h using a syringe pump (Harvard Apparatus, Holliston MA).

Cell association under static conditions: HUVECs were seeded at 40,000 cells per well in 48-well plates, incubated for 22 h at 37 °C, 5% CO_2. 240 µL of nanoparticles in EGM were added to the cells and incubated for 4 h. The cells were then washed three times with chilled HBSS and collected after treating with trypsin/EDTA (Lonza). After centrifugation at 300 g for 5 minutes, cells were resuspended in 300 µL of 1 mM propidium iodide (PI, Life Technologies) solution in HBSS, and analyzed by flow cytometry using a FACSCanto II (BD Biosciences, San Jose, CA).

Cell association under flow conditions: Nanoparticles in EGM were injected into the chip via a 1-mL syringe connected with Tygon tubing (0.02″ID x 0.06″OD, SynVivo). The flow of nanoparticles (in EGM) was perfused from the inlet port through the chip for 4 h at 1.0 µL min^{-1} using a syringe pump. At the end of the experiments, 1 mL of chilled HBSS was used to wash out non-associated particles. For quantifying cellular association using flow cytometry, HUVECs were treated with chilled trypsin/EDTA followed by incubating in a fridge at 4 °C for 5 minutes before harvesting. After that, the HUVECs were collected by centrifuging at 300 g for 5 minutes at 4 °C, and resuspended in 300 µL of 1 mM PI in HBSS. Cellular association of nanoparticles was then analyzed by flow cytometry (FACSCanto II from BD Biosciences, San Jose, CA*).* For live cell imaging, a solution of 1 mM Calcein AM (Sigma Aldrich) and 0.3 mM Hoechst 33342 (Sigma Aldrich) in HBSS was perfused through the chip for 15 minutes at 5 µl min^{-1}. After that, the device was incubated for another 10 minutes before acquiring images using a confocal microscope.

Supporting Information

Supporting Information is available from the Wiley Online Library or from the author.

Acknowledgements

‡ S. Y. Khor and M. N. Vu contributed equally to this work. Electron microscopy was performed at the Bio21 Advanced Microscopy Facility, The University of Melbourne. This work was carried out within the Australian Research Council (ARC) Centre of Excellence in Convergent Bio-Nano Science and Technology (Project No. CE140100036). We would like to thank Mr Cameron Nowell for his technical support on confocal microscopy. S.Y.K. acknowledges the financial support from the Australian Government Research Training Program Scholarship. M.N.V. acknowledges the financial support of Vietnamese Government and the Faculty of Pharmacy and Pharmaceutical Sciences, Monash University. N.P.T. acknowledges the award of a DECRA Fellowship from the ARC (DE180100076). J.F.Q. acknowledges receipt of a Future Fellowship from the ARC (FT170100144). T.P.D. is grateful for the award of an Australian Laureate Fellowship from the ARC (FL140100052).

Received: ((will be filled in by the editorial staff))
Revised: ((will be filled in by the editorial staff))
Published online: ((will be filled in by the editorial staff))

References

[1] M. E. Davis, Z. Chen, D. M. Shin, *Nat. Rev. Drug Discovery* **2008,** *7,* 771.

[2] D. Peer, J. M. Karp, S. Hong, O. C. Farokhzad, R. Margalit, R. Langer, *Nat. Nanotechnol.* **2007,** *2,* 751.

[3] N. P. Truong, J. F. Quinn, M. R. Whittaker, T. P. Davis, *Polym. Chem.* **2016,** *7,* 4295.

[4] N. P. Truong, W. Y. Gu, I. Prasadam, Z. F. Jia, R. Crawford, Y. Xiao, M. J. Monteiro, *Nat. Commun.* **2013,** *4,* 1902.

[5] C. J. Cheng, G. T. Tietjen, J. K. Saucier-Sawyer, W. M. Saltzman, *Nat. Rev. Drug Discovery* **2015,** *14,* 239.

[6] H. F. Yuan, W. Jiang, C. A. von Roemeling, Y. Q. Qie, X. J. Liu, Y. X. Chen, Y. F. Wang, R. E. Wharen, K. Yun, G. J. Bu, K. L. Knutson, B. Y. S. Kim, *Nat. Nanotechnol.* **2017,** *12,* 763.

[7] M. E. Lobatto, V. Fuster, Z. A. Fayad, W. J. M. Mulder, *Nat. Rev. Drug Discovery* **2011,** *10,* 835.

[8] C. Li, *Nat. Mater.* **2014,** *13,* 110.

[9] H. T. Ta, N. P. Truong, A. K. Whittaker, T. P. Davis, K. Peter, *Expert Opin. Drug Deliv.* **2017,** *15,* 33.

[10] N. P. Truong, M. R. Whittaker, C. W. Mak, T. P. Davis, *Expert Opin. Drug Deliv.* **2015,** *12,* 129.

[11] S.-Y. Lee, M. Ferrari, P. Decuzzi, *J. Biomech.* **2009,** *42,* 1885.

[12] R. Toy, P. M. Peiris, K. B. Ghaghada, E. Karathanasis, *Nanomed.* **2014,** *9,* 121.

[13] H. J. Hsieh, C. A. Liu, B. Huang, A. H. H. Tseng, D. L. Wang, *J. Biomed. Sci.* **2014,** *21*.

[14] M. Bjornmalm, M. Faria, X. Chen, J. W. Cui, F. Caruso, *Langmuir* **2016,** *32,* 10995.

[15] O. C. Farokhzad, A. Khademhosseini, S. Y. Yon, A. Hermann, J. J. Cheng, C. Chin, A. Kiselyuk, B. Teply, G. Eng, R. Langer, *Anal. Chem.* **2005,** *77,* 5453.

[16] S. P. Samuel, N. Jain, F. O'Dowd, T. Paul, D. Kashanin, V. A. Gerard, Y. K. Gun'ko, A. Prina-Mello, Y. Volkov, *Int. J. Nanomedicine* **2012,** *7,* 2943.

[17] B. Prabhakarpandian, M. C. Shen, K. Pant, M. F. Kiani, *Microvasc. Res.* **2011,** *82,* 210.

[18] G. Lamberti, Y. Tang, B. Prabhakarpandian, Y. Wang, K. Pant, M. F. Kiani, B. Wang, *Microvasc. Res.* **2013,** *89,* 107.

[19] B. Prabhakarpandian, K. Pant, R. C. Scott, C. B. Pattillo, D. Irimia, M. F. Kiani, S. Sundaram, *Biomed Microdevices* **2008,** *10,* 585.

[20] J. M. Rosano, N. Tousi, R. C. Scott, B. Krynska, V. Rizzo, B. Prabhakarpandian, K. Pant, S. Sundaram, M. F. Kiani, *Biomed Microdevices* **2009,** *11,* 1051.

[21] P. Kolhar, A. C. Anselmo, V. Gupta, K. Pant, B. Prabhakarpandian, E. Ruoslahti, S. Mitragotri, *Proc. Natl. Acad. Sci. U. S. A.* **2013,** *110,* 10753.

[22] N. Doshi, B. Prabhakarpandian, A. Rea-Ramsey, K. Pant, S. Sundaram, S. Mitragotri, *J. Controlled Release* **2010,** *146,* 196.

[23] Y. Tang, F. Soroush, J. B. Sheffield, B. Wang, B. Prabhakarpandian, M. F. Kiani, *Sci. Rep.* **2017,** *7, 9359.*

[24] B. Prabhakarpandian, M. C. Shen, J. B. Nichols, C. J. Garson, I. R. Mills, M. M. Matar, J. G. Fewell, K. Pant, *J. Controlled Release* **2015,** *201,* 49.

[25] N. P. Truong, J. F. Quinn, M. V. Dussert, N. B. T. Sousa, M. R. Whittaker, T. P. Davis, *ACS Macro Letters* **2015,** *4,* 381.

[26] N. P. Truong, C. Zhang, T. A. H. Nguyen, A. Anastasaki, M. W. Schulze, J. F. Quinn, A. K. Whittaker, C. J. Hawker, M. R. Whittaker, T. P. Davis, *ACS Macro Letters* **2018,** *7,* 159.

[27] L. Esser, N. P. Truong, B. Karagoz, B. A. Moffat, C. Boyer, J. F. Quinn, M. R. Whittaker, T. P. Davis, *Polym. Chem.* **2016,** *7,* 7325.

[28] N. P. Truong, M. R. Whittaker, A. Anastasaki, D. M. Haddleton, J. F. Quinn, T. P. Davis, *Polym. Chem.* **2016,** *7,* 430.

[29] N. P. Truong, J. F. Quinn, A. Anastasaki, D. M. Haddleton, M. R. Whittaker, T. P. Davis, *Chem. Commun.* **2016,** *52,* 4497.

[30] S. Kaga, N. P. Truong, L. Esser, D. Senyschyn, A. Sanyal, R. Sanyal, J. F. Quinn, T. P. Davis, L. M. Kaminskas, M. R. Whittaker, *Biomacromolecules* **2017,** *18,* 3963.

[31] N. G. Engelis, A. Anastasaki, G. Nurumbetov, N. P. Truong, V. Nikolaou, A. Shegiwal, M. R. Whittaker, T. P. Davis, D. M. Haddleton, *Nat. Chem.* **2016,** *9,* 171.

[32] N. P. Truong, J. F. Quinn, A. Anastasaki, M. Rolland, M. Vu, D. Haddleton, M. R. Whittaker, T. P. Davis, *Polym. Chem.* **2017,** *8,* 1353.

[33] N. P. Truong, M. V. Dussert, M. R. Whittaker, J. F. Quinn, T. P. Davis, *Polym. Chem.* **2015,** *6,* 3865.

[34] S. Y. Khor, N. P. Truong, J. F. Quinn, M. R. Whittaker, T. P. Davis, *ACS Macro Letters* **2017,** *6,* 1013.

[35] J. Rosselgong, A. Blanazs, P. Chambon, M. Williams, M. Semsarilar, J. Madsen, G. Battaglia, S. P. Armes, *Acs Macro Letters* **2012,** *1,* 1041.

[36] C. Grazon, J. Rieger, R. Meallet-Renault, B. Charleux, G. Clavier, *Macromolecules* **2013,** *46,* 5167.

[37] M. Zamfir, J. F. Lutz, *Nat. Commun.* **2012,** *3*.

[38] B. V. K. J. Schmidt, N. Fechler, J. Falkenhagen, J. F. Lutz, *Nat. Chem.* **2011,** *3,* 234.

[39] C. Freese, L. Anspach, R. C. Deller, S. J. Richards, M. I. Gibson, C. J. Kirkpatrick, R. E. Unger, *Biomater Sci-Uk* **2017,** *5,* 707.

[40] J. W. Cui, M. Faria, M. Bjornmalm, Y. Ju, T. Suma, S. T. Gunawan, J. J. Richardson, H. Heidar, S. Bals, E. J. Crampin, F. Caruso, *Langmuir* **2016,** *32,* 12394.

[41] N. P. Truong, Z. Jia, M. Burges, N. A. McMillan, M. J. Monteiro, *Biomacromolecules* **2011,** *12,* 1876.

[42] N. P. Truong, Z. F. Jia, M. Burgess, L. Payne, N. A. J. McMillan, M. J. Monteiro, *Biomacromolecules* **2011,** *12,* 3540.

[43] M. S. Ehrenberg, A. E. Friedman, J. N. Finkelstein, G. Oberdorster, J. L. McGrath, *Biomaterials* **2009,** *30,* 603.

[44] N. Faucheux, R. Schweiss, K. Lutzow, C. Werner, T. Groth, *Biomaterials* **2004,** *25,* 2721.

[45] E. C. Eckstein, A. W. Tilles, F. J. Millero, *Microvasc. Res.* **1988,** *36,* 31.

[46] T. R. Lee, M. Choi, A. M. Kopacz, S. H. Yun, W. K. Liu, P. Decuzzi, *Sci Rep-Uk* **2013,** *3*.

[47] H. Y. Liu, A. P. R. Johnston, *Angew. Chem. Int. Edit.* **2013,** *52,* 5744.

[48] J. F. Tan, S. Shah, A. Thomas, H. D. Ou-Yang, Y. L. Liu, *Microfluid Nanofluid* **2013,** *14,* 77.

[49] C. Fillafer, G. Ratzinger, J. Neumann, Z. Guttenberg, S. Dissauer, I. K. Lichtscheidl, M. Wirth, F. Gabor, M. F. Schneider, *Lab Chip* **2009,** *9,* 2782.

[50] V. R. S. Patil, C. J. Campbell, Y. H. Yun, S. M. Slack, D. J. Goetz, *Biophys. J.* **2001,** *80,* 1733.

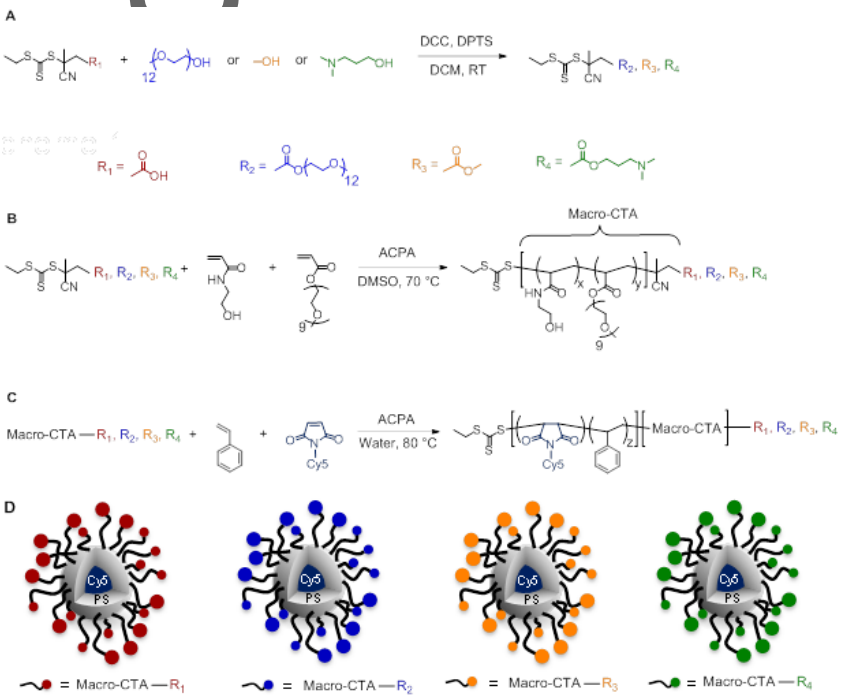

Scheme 1. (A) Modification of the ECT; (B) RAFT solution polymerization of HEAA and PEGA; (C) Aqueous RAFT emulsion polymerization of styrene and Cy5-maleimide; (D) Schematic representation of particles with different end-groups formed via PISA.

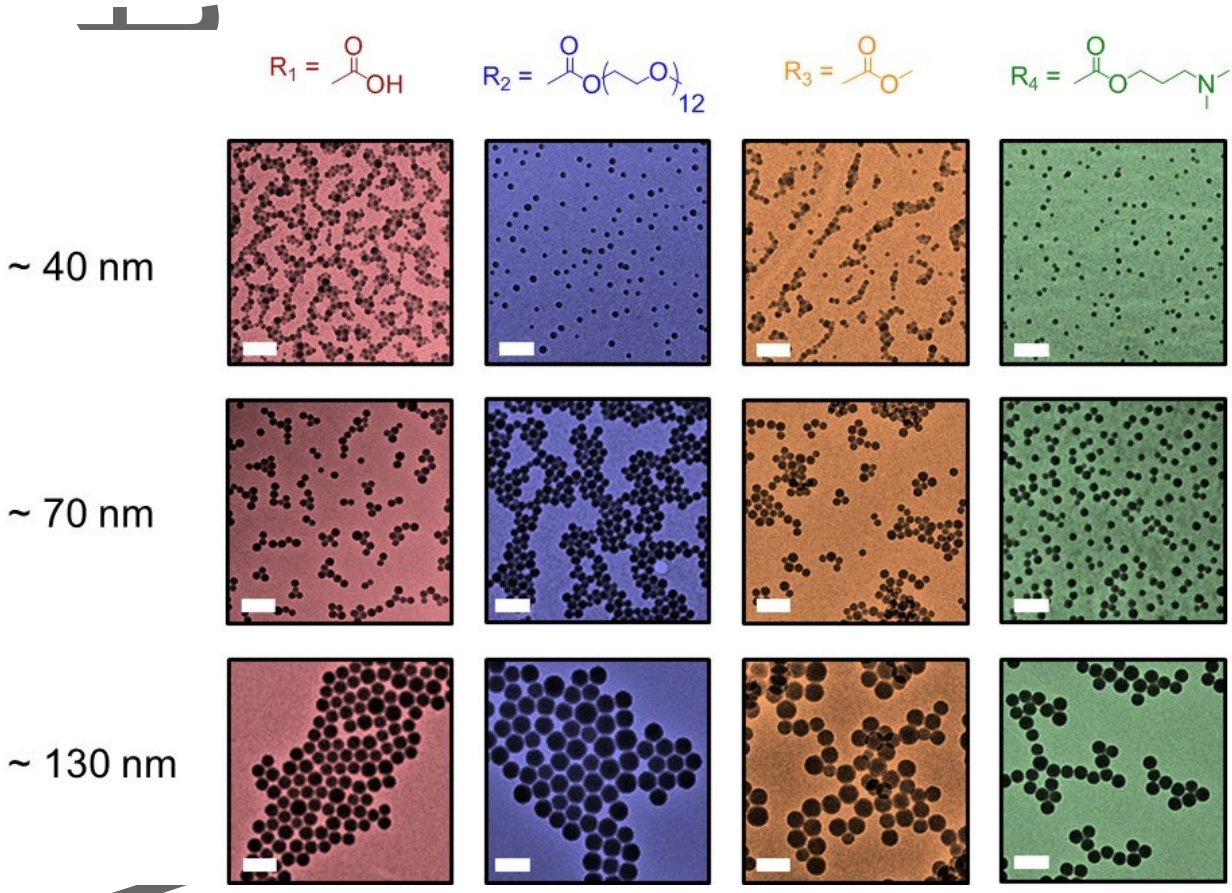

Figure 1. TEM images of the nanoparticles obtained by RAFT aqueous emulsion polymerization of styrene with (red) P(HEAA-*co*-PEGA)-COOH, (blue) P(HEAA-*co*-PEGA)-N(CH_3)$_2$, (green) P(HEAA-*co*-PEGA)-Me, and (yellow) P(HEAA-*co*-PEGA)-PEG, at 80 °C for 6 h. All scale bars represent 200 nm.

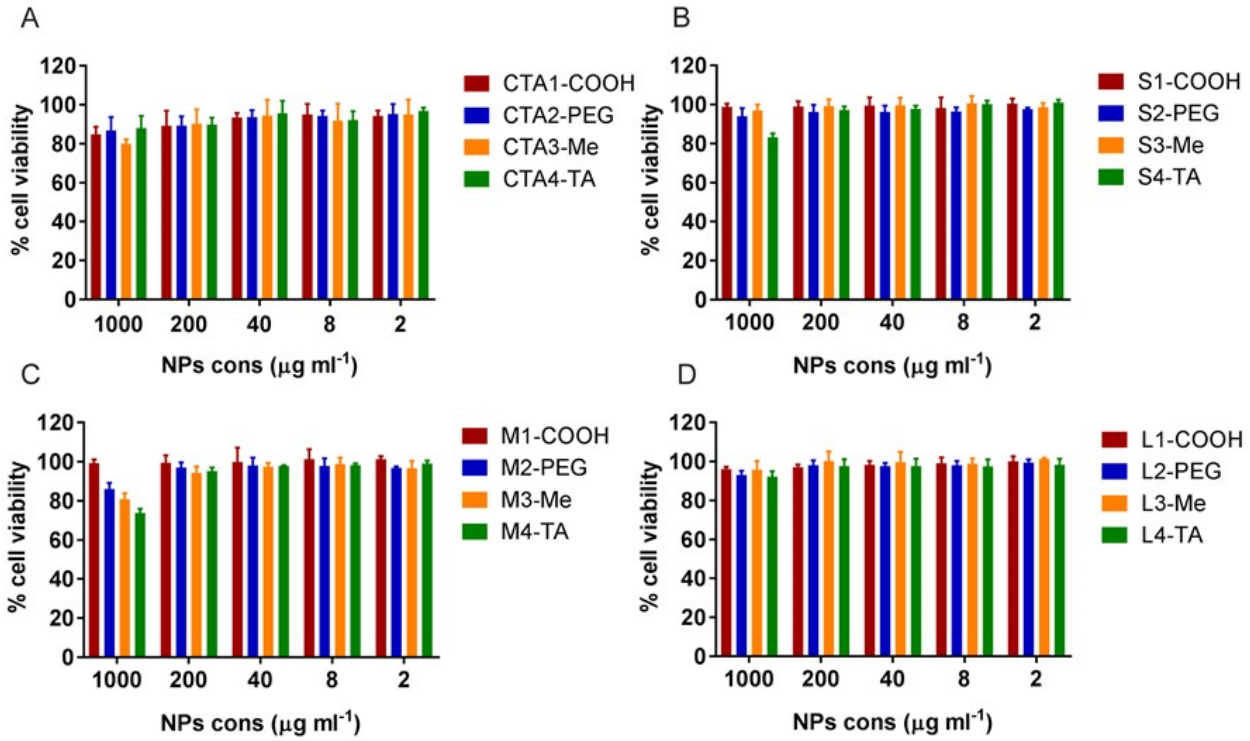

Figure 2. Evaluation of cytotoxicity to HUVECs after 48 h for (A) macro-CTAs, (B) small particles, (C) intermediate particles, and (D) large particles under static conditions using AlamarBlue assay for 48 h. Data are shown as mean ± SD (n = 3).

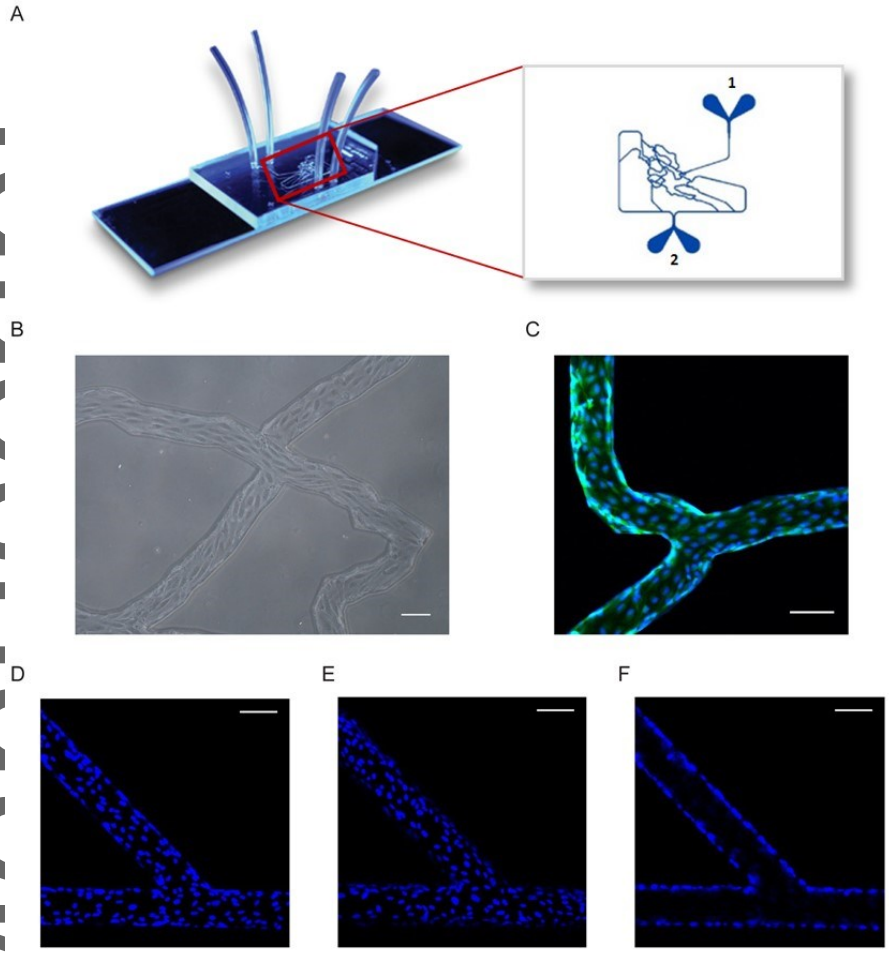

Figure 3. (A) Model synthetic microvascular network, adapted from SynVivo website: (1) Inlet port where cell growth media with or without nanoparticles is injected into the system and (2) Outlet port where perfusate from the system is collected; (B) Bright field and (C) confocal images of a confluent layer of HUVECs in flow channels. Cells were stained with Calcein AM (cytoplasm – green channel) and Hoechst 33342 (nucleus – blue channel). (D-F) Nucleus of HUVECs stained with Hoechst 33342 was imaged at the bottom (D), at the top (E), and on the sides (F) of the vascular pipeline. Scale bars = 100 μm.

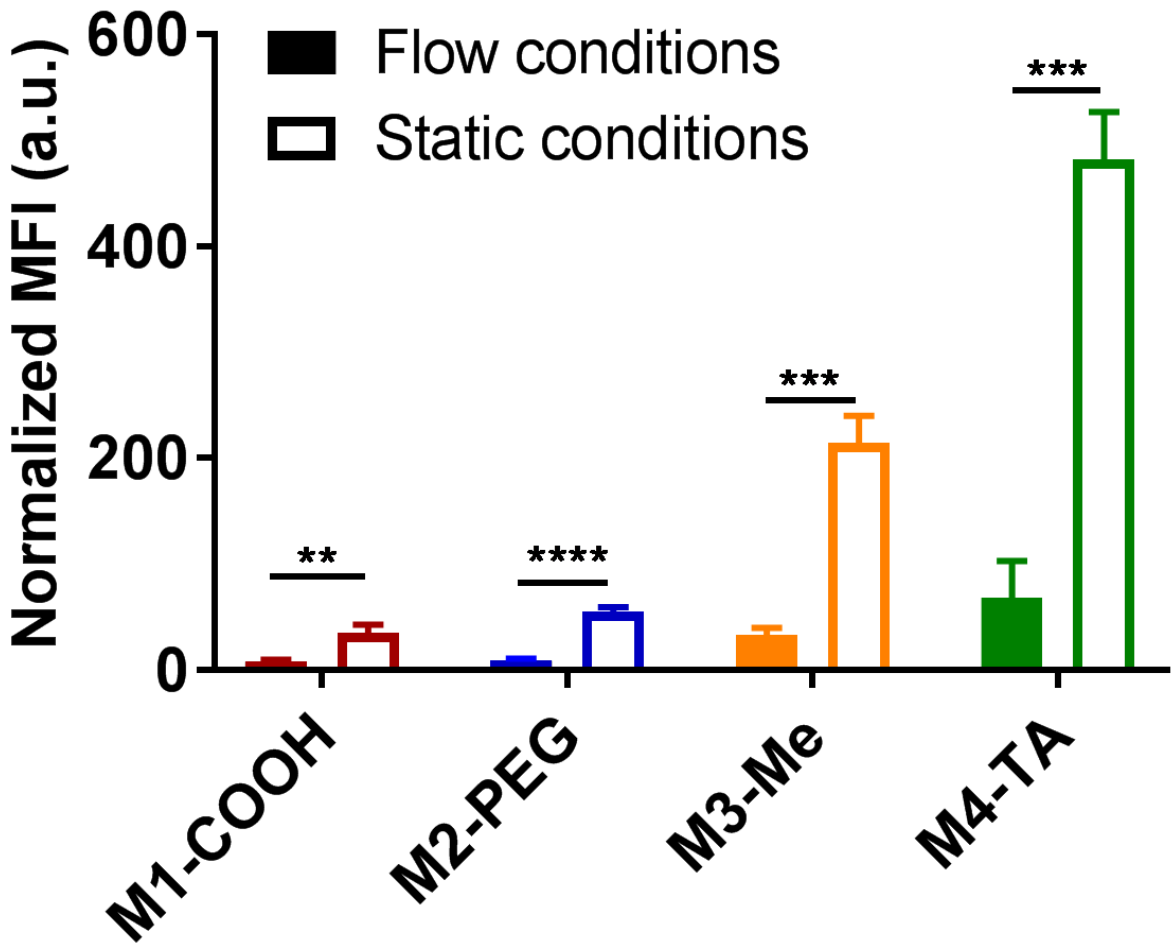

Figure 4. Cellular association of four different end-group particles with HUVECs under static and flow conditions as measured by flow cytometry. Data are presented as with mean ± SD (n = 3); ** $P <$ 0.01, *** $P < 0.001$, **** $P < 0.0001$ (pair *t*-test).

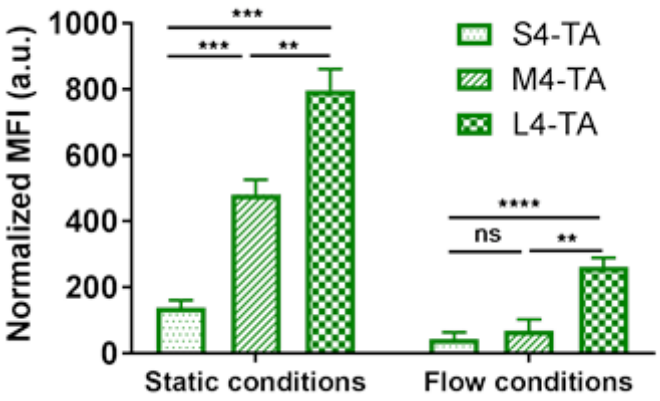

.

Figure 5. Cellular association of amine-functionalized particles having three different sizes with HUVECs under static and flow conditions as measured by flow cytometry. Data are presented as mean ± SD (n = 3), ** $P < 0.01$, *** $P < 0.001$, **** $P < 0.0001$, ns $P > 0.05$ (pair *t*-test).

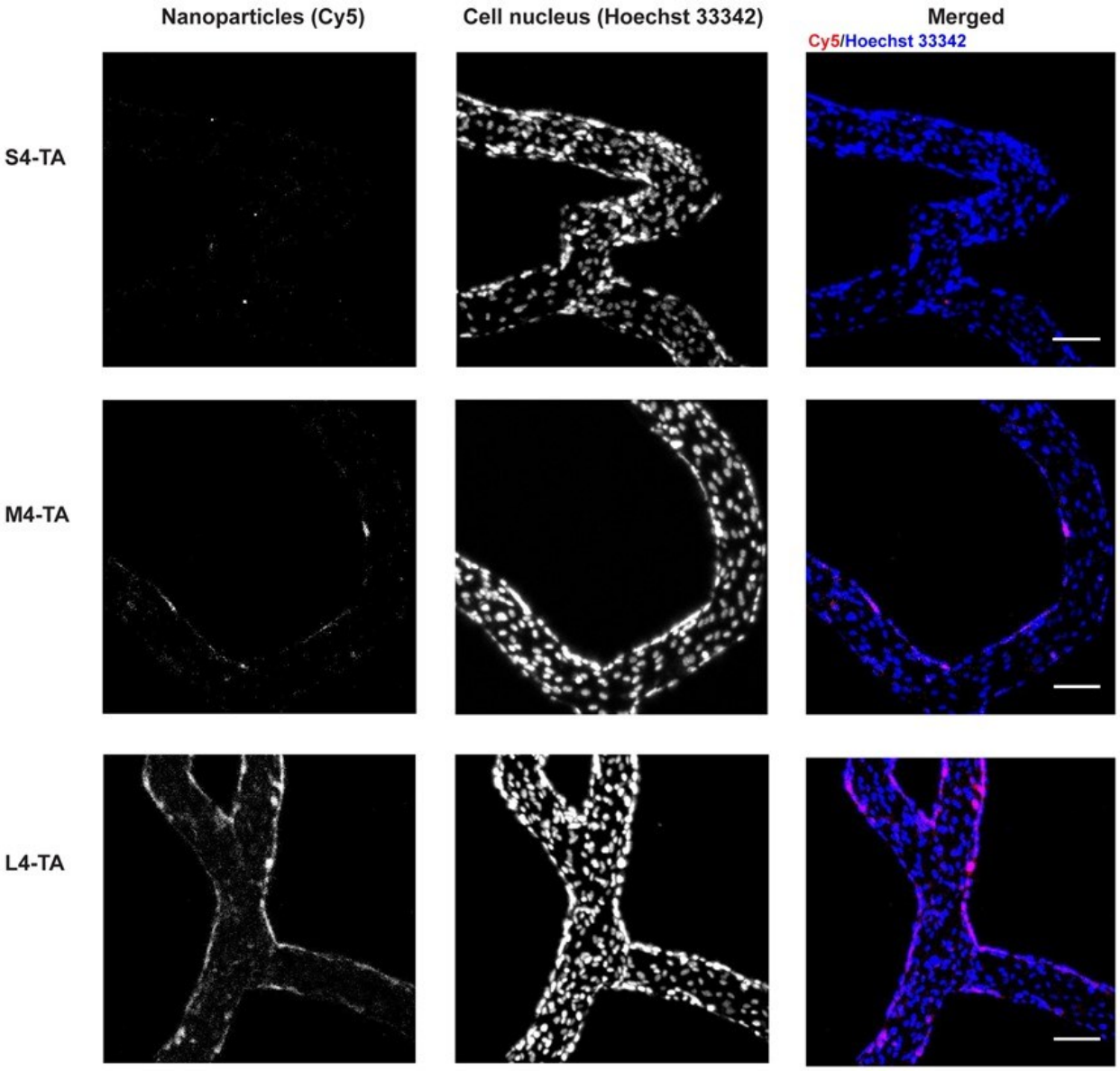

Figure 6. Images of tertiary amine-functionalized particles with three different sizes associated with HUVECs in the synthetic vascular network. Scale bars = 100 μm.

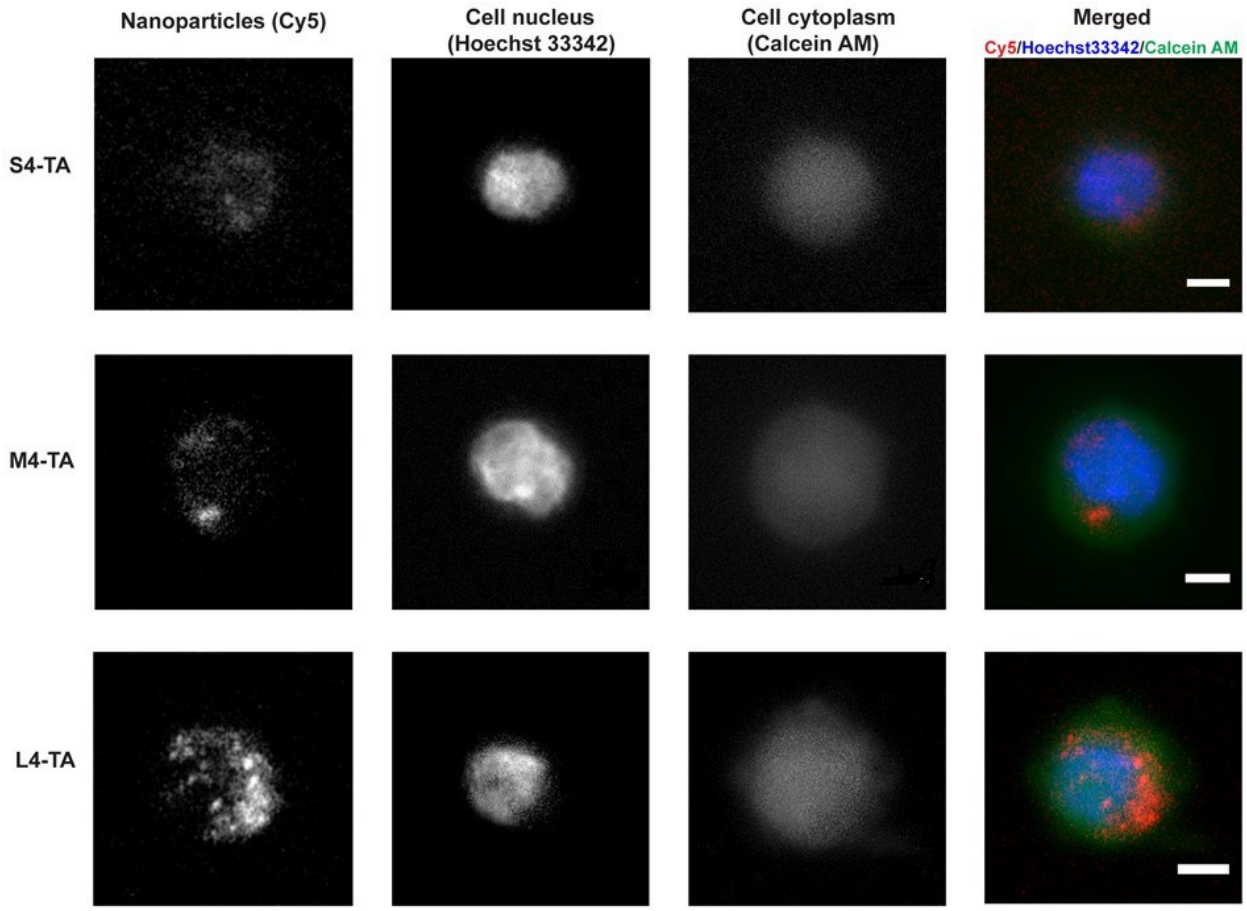

Figure 7. Images of tertiary amine-functionalized particles with three different sizes internalized into HUVECs under flow conditions. The cells were harvested from the vascular network, mounted onto coverslips, and imaged using a Nikon A1R confocal microscope. Scale bars = 5 μm.

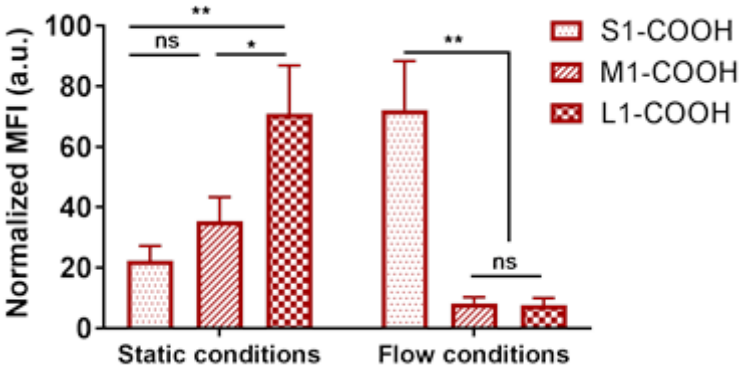

Figure 8. Cellular association between carboxylic acid-functionalized particles with three different sizes and HUVECs under static and flow conditions as measured by flow cytometry. Data are presented as mean ± SD (n = 3); * $P < 0.05$, ** $P < 0.01$, ns $P > 0.05$ (pair *t*-test).

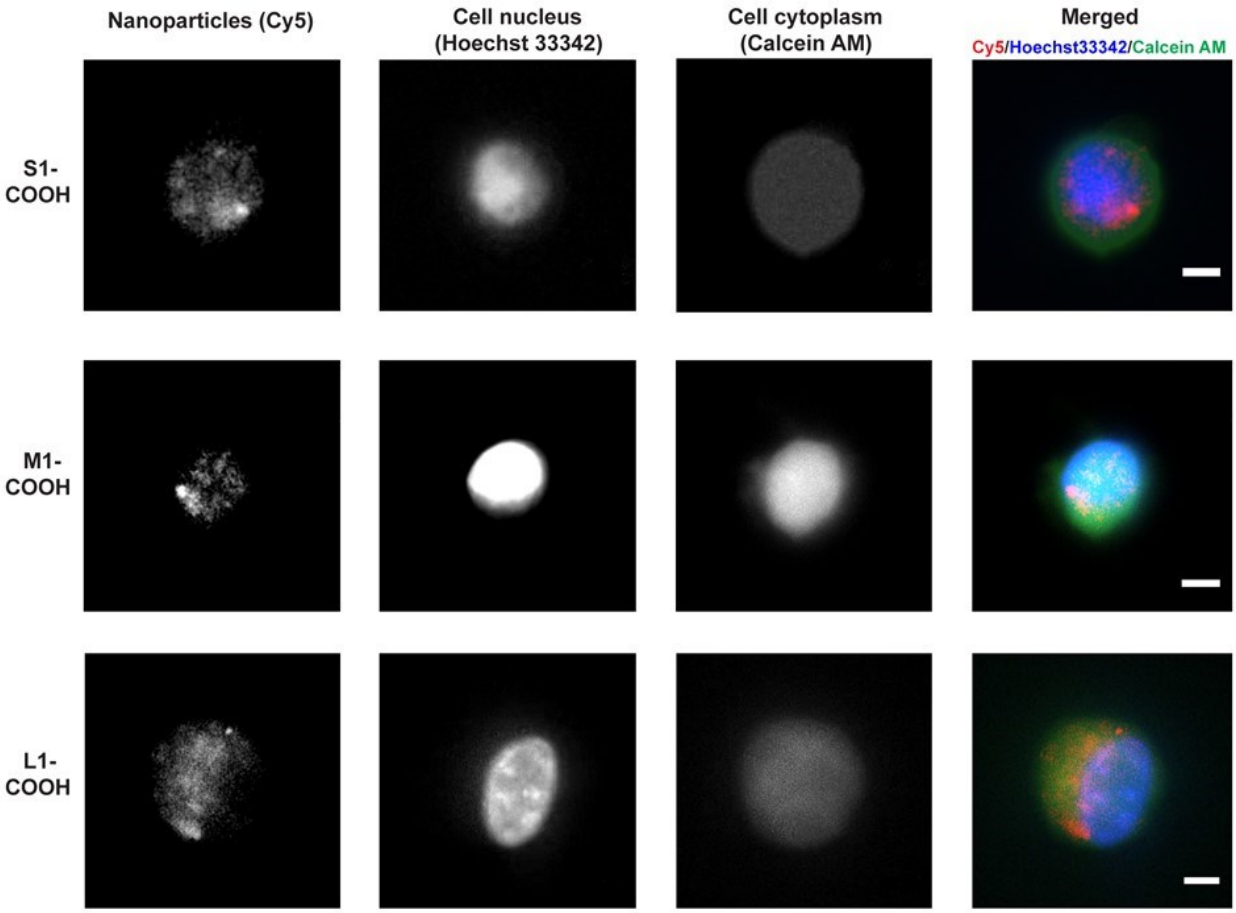

Figure 9. Images of carboxylic acid-functionalized particles with three different sizes internalized into HUVECs under flow conditions. The cells were harvested from the vascular network, mounted onto coverslips, and imaged using a Nikon A1R confocal microscope. Scale bars 5 μm.

The table of contents: A novel facile and versatile polymerization-induced self-assembly technique has been developed to produce fluorescent nanoparticles with various sizes and surface chemistries. An advanced biological characterization method based on a synthetic microvascular network embedded in a microfluidic device elucidates the interplay of nanoparticle physicochemical properties and dynamic flow.

Keywords: dynamic flow, size, surface chemistry, cellular association, PISA

Song Yang Khor‡, Mai N. Vu‡, Emily H. Pilkington, Angus P.R.Johnston, Michael R. Whittaker, John F. Quinn, Nghia P. Truong, and Thomas P. Davis**

Elucidating the influences of size, surface chemistry and dynamic flow on cellular association of nanoparticles made by polymerization-induced self-assembly

ToC figure